Separation and Purification Technology 240 (2020) 116614

Contents lists available at ScienceDirect

Separation and Purification Technology

journal homepage: www.elsevier.com/locate/seppur

Phosphorus separation from metallurgical-grade silicon by magnesium alloying and acid leaching

Mengyi Zhu[a], Alexander Azarov[b], Eduard Monakhov[b], Kai Tang[c], Jafar Safarian[a,*]

[a] Department of Materials Science and Engineering, Norwegian University of Science and Technology (NTNU), Trondheim, Norway
[b] Centre for Materials Science and Nanotechnology, Department of Physics, University of Oslo, P.O. Box 1048 Blindern, N-0316 Oslo, Norway
[c] SINTEF Materials and Chemistry, N-7465 Trondheim, Norway

ARTICLE INFO

Keywords:
Metallurgical grade silicon
Purification
Acid leaching
Phosphorus
Impurities

ABSTRACT

In this paper, the separation of phosphorus from metallurgical-grade silicon was investigated based on an Mg alloying and HCl leaching approach. Experimental results show that P concentration was reduced from initial 15.1 ppmw to 0.2 ppmw with also large extent removal of metallic impurities by two times Mg alloying-leaching purification. The mechanism of enhanced P separation is clarified owing to the strong affinity between Mg and P, which is validated by SIMS elemental mapping. A two-parameter analytical model was developed to predict the P removal degree based on the variables of alloying metal concentration and interaction coefficient between alloying metal and P. The model is validated with experimental results and the interaction coefficient $\varepsilon^{P}_{Mg\ in\ Si}$ was obtained as −10.8. This approach can be applied to model the removal of impurity which follows Gulliver-Scheil solidification from other binary alloying systems. Furthermore, in order to study the effect of applied alloying-leaching operation times, a model was proposed which establishes the mathematical relationships among key processing variables like initial and target P concentrations, the amount of the alloying metal, and the process operation times.

1. Introduction

The rapid growth of the photovoltaic industry worldwide has given rise to large demands of solar grade silicon (SoG-Si, purity 99.9999%) feedstock production. The metallurgical route for SoG-Si production has, therefore, become an emerging technology due to its large production capacity, low-cost, and environment-friendly features [1,2]. However, the main challenge of the metallurgical route for SoG-Si production is the removal of large concentration of impurities from the raw material metallurgical grade silicon (MG-Si, 99% Si), especially the removal B and P, which are the major important impurities for the solar cells. In the commercialized Elkem Solar metallurgical process operated by REC Solar Norway, MG-Si is purified through the combination of slag refining, acid leaching, and directional solidification [2]. As one of the crucial steps, the task of acid leaching is aiming at removing large extent metallic impurities, and, more importantly, to reduce the P concentration down to 0.1–0.3 ppmw to meet the restricted high-purity requirement of SoG-Si.

The research of silicon purification by acid leaching has been carried out over decades in respect of determining optimum leaching conditions [3–7], precipitated phase reactivity [8–10], and leaching kinetics [11,12]. However, it is generally accepted that only parts of P and metallic impurities can be removed due to the weak segregation and low chemical reactivity of the Fe-bearing precipitates. In order to further improve the impurity removal efficiency, new method has emerged to purify Si by means of introducing new alloying element to modify the impurity segregation behavior during solidification. One typical example is the widely known solvent refining [13,14], which mainly relies on a large amount of alloying metal addition like Al [15–24], Sn [24–28], Cu [29–31], and Fe [32] and so on. In this way, low operation temperature can be achieved for lower process energy consumption, but the large amount of the alloying metal addition causes high cost of the process. Unlike solvent refining, the addition of only small amount of more reactive alloying elements into Si melt brings more economic benefits and also reaches high impurity removal degree. Schei et al. [33] investigated the effect of Ca addition on impurities removal and found that the impurities embedded inside a leachable $CaSi_2$ phase. Shimpo et al. [34] investigated the thermodynamic interaction between Ca and P, and confirmed Ca has a strong affinity to P in molten Si. Other researchers also reported high P removal degree after Ca alloying [35–39], but the difficulty of separating viscous byproduct siloxene still remains challenging [1]. Alternative

* Corresponding author.
E-mail address: Jafar.Safarian@ntnu.no (J. Safarian).

https://doi.org/10.1016/j.seppur.2020.116614
Received 17 October 2019; Received in revised form 7 January 2020; Accepted 21 January 2020
Available online 25 January 2020

Table 1
Composition of starting materials before acid leaching (in ppmw).

	S1 MG-Si	S2 Si-2.2 wt% Mg	S3 Si-5.5 wt% Mg	S4 Si-1.8 wt% Mg	S5 Si-3.8w%Mg	Re-alloyed S3 4 wt%Mg
B	46.2	44.9	44.3	19.5	18.9	44.0
P	15.8	12.2	15.1	4.4	3.9	3.4
Mg	9.6	19424.9	54804.5	17908.9	37774.8	41251.5
Ca	266.7	252.2	267.0	73.3	97.9	26.8
Al	2548.0	259.8	1717.8	610.2	618.8	207.4
Fe	3167.5	1619.3	2154.0	948.1	966.4	1014.8
Ti	299.8	138.4	190.4	67.8	66.4	74.0
Mn	70.4	34.6	49.8	16.8	17.8	18.2
Zr	10.7	5.5	7.2	2.7	2.7	4.1
Si	Balance	Balance	Balance	Balance	Balance	Balance

alloying elements such as Ti [35], Hf [40], Zr [41], have been also studied for different purposes and with their own features, but they are not feasible to be used in practice due to the high prices of these metals and the difficulties in their further removal for solar silicon production.

In this work, a comprehensive study of novel Mg alloyed MG-Si acid leaching was conducted according to the attractive features exhibited by the Mg alloying in our recent research works [42–44]. Various parameters such as acid concentration, leaching time, and Mg addition amount are studied to validate the applicability of Mg alloying on impurities removal. Moreover, two theoretical models were proposed to better understand the P removal via the Si alloying-leaching process.

2. Materials and methods

2.1. Materials

A commercial MG-Si was selected as the starting material, the detailed composition can be seen in Table 1. High purity (99.8%, Alfa Aesar) Mg rod with low P concentration was cut into pieces used for MG-Si alloying. Analytical grade reagents hydrochloric acid (HCl) was supplied by VWR International. The concentrated HCl aqueous solution was diluted by deionized water to obtain different concentration for leaching trials.

2.2. Silicon alloying by Mg and leaching

The alloying and leaching process of MG-Si purification can be seen in Fig. 1. MG-Si lumps were first carefully put into a graphite crucible with ultra-high purity. The crucible was then placed in an induction furnace. Before heating, the furnace chamber was evacuated to high vacuum and then re-filled by pure Argon gas to 1 atm followed by continuous Ar flow. MG-Si lumps were subsequently heated up to 1500 °C as molten state. Specific amount of Mg piece was then added into the melt for targeting alloy composition. After Mg addition, the molten alloy was slowly cooled down and solidified under the same condition inside the furnace chamber. It is worth noting that even though P has a high vapor pressure, but the P loss caused by evaporation can be ignored due to the ultra-low activity and short melting time.[45,46] The obtained Si-Mg alloy was then crushed and sieved to specific particle size (0.2–1 mm) for the following acid leaching. The chemical compositions of MG-Si and Mg-doped samples were measured by high-resolution Inductively Coupled Plasma-Mass Spectroscopy (ICP-MS, Thermo Scientific Element 2, US) are listed in Table 1.

Table 2
Detailed conditions of performed leaching trials.

ID	Si source	HCl Concentration	Leaching Time (h)	Leaching Temperature (°C)	Leaching method
L1	S1	10%	3	60	M
L2	S2	5%	5	60	M
L3		10%	5	60	M
L4		15%	5	60	M
L5		20%	5	60	M
L6	S3	10%	0.5	60	M
L7			1	60	M
L8			2	60	M
L9			3	60	M
L10	Re-	10%	0.5	60	M
L11	alloyed		1	60	M
L12	S3		2	60	M
L13			3	60	M
L14	S2	10%	3	60	U
L15	S3	10%	3	60	U
L16	S4	10%	3	60	U
L17	S5	10%	3	60	U

A number of leaching trials were designed for different research purposes as shown in Table 2. Herein, the leaching trials and conditions are determined based on our preliminary work [42–44]. For the magnetic-stirrer leaching (M), 100 g fine particle sample was placed in a 500 mL Pyrex beaker with 250 mL 10% HCl preheated at 60 °C on hotplate. A total leaching period up to 3 h was performed using a magnetic stirring condition with 200 rpm. For the ultrasonic leaching trials (U), 2 g sample with 10 mL 10%HCl was mixed in perfluoroalkoxy alkane (PFA) bottle and then put into ultrasonic bath with the same temperature as the magnetic-stirrer leaching. After leaching, the remaining particles were washed by distilled water and dried. Ultra-fine particles were sieved by a 100 μm sieve before analysis in order to reduce the interference of undissolved metallic impurities.

2.3. Characterization

The MG-Si material and produced Si-Mg alloys were analyzed by a Secondary Electron Microscope (SEM, Hitachi SU6600, Japan) with Energy Dispersive X-ray Spectrometry (EDS) detector to study the microstructure variation. The chemical composition of all the samples after leaching was measured by the high-resolution ICP-MS. A magnetic sector Secondary Ion Mass Spectrometry (SIMS) instrument (CAMECA IMS 7f) was employed to analyze the P distribution in Mg alloyed samples. The SIMS measurements were performed in the imaging mode using 15 keV Cs^+ ions as a primary beam rastered over the area of 500 × 500 μm^2. The beam current was kept at 1nA during the measurements.

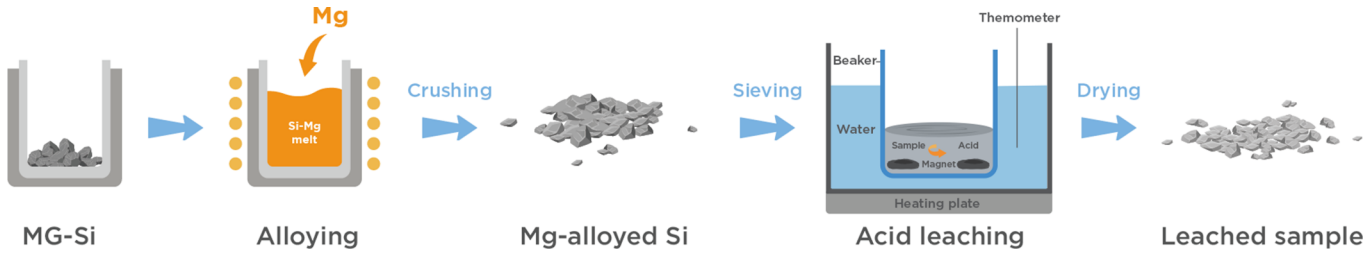

Fig. 1. Schematic of the Mg alloying and acid leaching process.

3. Results

3.1. Microstructure

Before acid leaching, the microstructure of sample S1, S2, S3, and Re-alloyed S3 was analyzed by SEM and shown in Fig. 2. A number of precipitated phases are observed, and the chemical composition was further analyzed by EDS.

In Fig. 2(a and b) of the raw MG-Si sample Si, the identified precipitates are mainly as Fe-bearing silicide, respectively, $CaAl_6Fe_4Si_8$, Al_3FeSi_2, $TiFeSi_2$, and $FeSi_{2.4}$.

The effect of Mg alloying on the microstructure of MG-Si can be observed in Fig. 2(c–f). A large amount of eutectic Mg_2Si phase can be distinctly observed in both of the Mg-alloyed samples. In sample S3, there is also some eutectic silicon phase observed in Mg_2Si, while in the sample S2 much less eutectic silicon was found. In addition, the Fe-bearing silicide phases were found embedded inside the Mg_2Si phase. Meanwhile, the $TiFeSi_2$ phase was also found in the Mg_2Si phase rather than in the $CaAl_6Fe_4Si_8$ phase as in MG-Si. The $CaAl_2Si_2$ phase was found in the Mg-alloyed samples as well.

For the leached and re-alloyed S3 sample, it can be seen from Fig. 2(g–h) that the eutectic Mg_2Si is still the main precipitate, but the content of the other impurities is much lower than that in sample S3. It can be also seen that Ca-bearing phase barely exists, and only a very

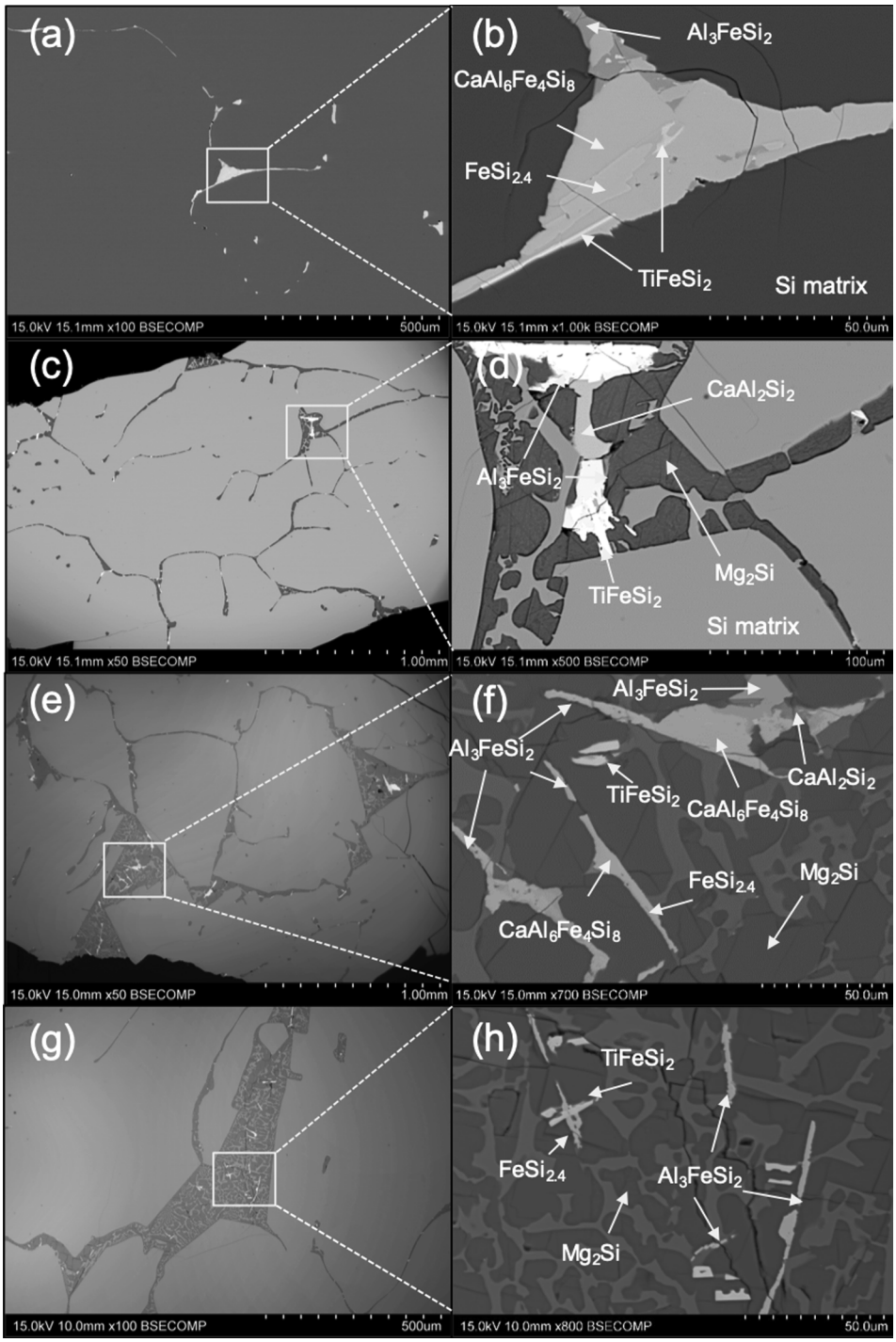

Fig. 2. Microstructure of precipitated phases in samples: (a–b) S1 (MG-Si); (c–d) S2 (Si-2.2 wt%Mg); (e–f) S3 (Si-5.5 wt%Mg), and (g–h) leached and re-alloyed S3.

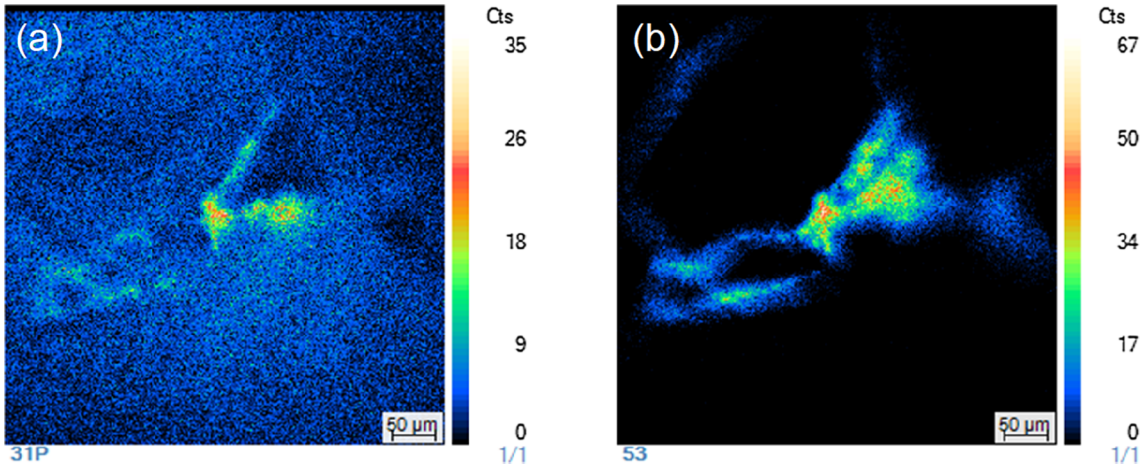

Fig. 3. SIMS mapping of (a) P distribution signal and (b) Mg + Si signal of sample S2 (Si-2.2 wt%Mg).

small amount of Al-bearing was found. The main impurity phases embedded inside Mg_2Si were determined as $TiFeSi_2$ and $FeSi_{2.4}$.

3.2. Phosphorus distribution

In order to detect the P distribution in Si-Mg alloy system, SIMS mapping analysis was performed as normal EDS analysis results for very low concentrations at ppm level are not reliable. The mapping images in Fig. 3 show a distinct enrichment of P signal in the Mg-alloyed Si sample S2. Moreover, the P signal is found partially overlapped with the signal of "Mg + Si" and close to the Mg_2Si/Si interface, which confirms the attraction of Mg to P and the enhanced P segregation in the Mg-alloyed Si subsequently.

3.3. Phase sensitivity to acid

A metallographic sample of S2 was leached three times in 10% HCl solution at 60 °C within total time period 0.2 h, 0.5 h, and 1 h to study the precipitated phase sensitivity to the acid solution. The microstructure evolution at each leaching trial was captured by SEM and the results are shown in Fig. 4.

It can be seen in Fig. 4 that the removal of the precipitated phase increases visibly with increasing leaching time. After 0.2 h leaching, most of the $CaAl_2Si_2$ phase was leached away and some of the $CaAl_6Fe_4Si_8$ phase was also removed in the short period. In addition, most of the Mg_2Si phase was dissolved into to aqueous acid solution and a distinct cracking effect was observed as well. After 0.5 h leaching, more of the Al_3FeSi_2 and $FeSi_{2.4}$ phases were dissolved. After 1 h leaching, a majority of precipitated phases were significantly removed except the insoluble $TiFeSi_2$ phase. A reactivity sequence of precipitates in Mg-alloyed MG-Si is subsequently obtained according to the metallographic sample leaching results:

$$CaAl_2Si_2,\ CaAl_6Fe_4Si_8 \ > \ Mg_2Si \gg Al_3FeSi_2,\ FeSi_{2.4} \ > \ TiFeSi_2$$

3.4. Variation of acid concentration

The impurity removal efficiency is expected to depend on the acid leaching conditions. As shown in Fig. 5, by plotting the leaching results as a function of acid concentration, a well-defined maximum can be observed at around 10% HCl that neither higher concentration nor lower HCl concentration improves the impurity removal degree. Here the removal degree of the impurities is calculated as:

$$Impurity\ \ removal\ \ degree = \frac{C_{Initial} - C_{Purified}}{C_{Initial}} \times 100\% \quad (1)$$

where $C_{Initial}$ and $C_{Purified}$ are the overall impurity concentration of samples before and after leaching in weight percent, respectively.

Since all the leaching trials were performed within the same time period, the different results thus indicate the difference of reaction kinetics with respect to different acid concentrations. More details are discussed in Section 4.1.

3.5. Re-alloying and re-leaching

Two sets of acid leaching trials (L6-L9 and L10-L13) were performed under constant conditions (60 °C, 10%HCl, magnetic stirring) to compare the effect of alloying-leaching times on impurities removal. The sample of the first leaching set is Mg-alloyed MG-Si sample S3. In the second leaching set, the sample is from the former 3 h leached S3 sample and re-alloyed by 4 wt% Mg once again. Samples used for ICP-MS measurement were subsequently taken at different leaching time of 0.5 h, 1 h, 2 h, and 3 h, respectively. Results can be seen in Fig. 6.

In the first leaching set (L6-L9), it is obvious that the concentration of the metallic impurities (Mg, Ca, Al, Fe, Ti, Mn, Zr) are decreases with increasing leaching time, especially in the first 1 h of acid leaching. P amount is also effectively reduced from 15.1 ppmw to 5.4 ppmw within 1 h leaching and further reduced to 5.1 ppmw after the first 3 h acid leaching for the sample S3. The exception is the removal of B, which has a high segregation coefficient ($k_B = 0.8$ [47]) in Si, and is generally considered to be not removed by the leaching method.

In the second leaching set of the Mg re-alloyed sample (L10-L13), a similar trend was observed again that most impurities were removed as the leaching process continues. More importantly, the concentration of impurities significantly reduced compares to the first leaching set. Furthermore, it was detected that P concentration after leaching successfully reduced to 0.2 ppmw, which meets the restricted requirements of the SoG-Si standard (P < 0.3 ppmw). Hence, the Mg alloying and re-alloying method exhibits a promising potential for the practical applications of MG-Si purification.

In order to further compare the leaching performance of the different alloying-leaching methods, the purification degree is calculated as below:

$$Purification\ \ degree = \frac{C_{MG-Si} - C_{Purified}}{C_{MG-Si}} \times 100\% \quad (2)$$

where the C_{MG-Si} and $C_{Purified}$ are impurity concentration of raw material MG-Si and after purification in weight percent.

The purification degree of studied three samples can be seen in Fig. 7. It can be observed that the purification efficiency follows the trend: direct MG-Si leaching < 1-time Mg alloying-leaching < 2-time Mg alloying. For sample S1, direct leaching of MG-Si, only limited P

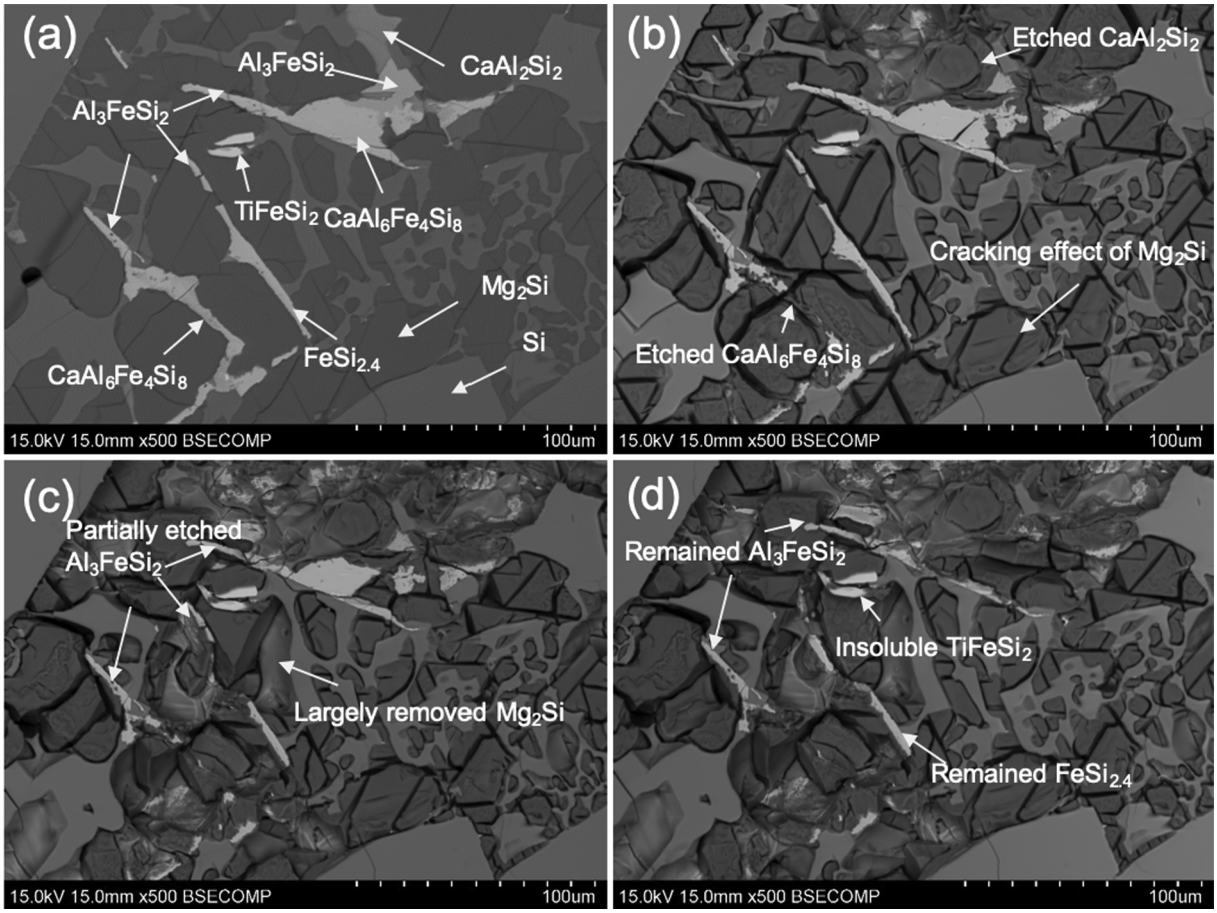

Fig. 4. Microstructure of sample S2 before leaching (a), and after acid leaching at 60 °C at (b) 0.2 h; (c) 0.5 h; (d) 1 h times by 10% HCl.

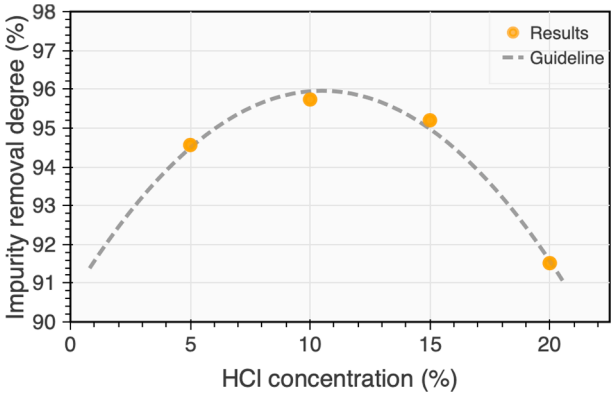

Fig. 5. Relationship between HCl concentration and the overall impurity removal degree from leaching trials L2-L5.

purification is achieved. The P purification degree is significantly improved from 31.1% to 69.5% after Mg alloying, and especially for the leached and re-alloyed S3 sample, nearly complete P removal is achieved. Moreover, for the purification of metallic impurities such as Ca, Al, Fe, Ti, Mn, and Zr, distinguished improvement can be observed as well by the re-alloying method.

4. Discussion

4.1. Mechanism of impurities removal

Based on the microscopic examinations and the leaching behavior of the phases, the mechanism of impurity removal for both MG-Si and Mg-doped Si samples by acid leaching can be explained as schematically illustrated in Fig. 8.

In MG-Si, it is known that the precipitates are mainly Fe-bearing silicide phases with poor leaching ability. In addition, these Fe-bearing silicides dispersed unevenly and usually with fine microstructure at the grain boundaries. When the leaching process starts, only a portion of these particles can be exposed to acid, and only small parts of them can be dissolved due to the limited reactivity, which is depending on process characteristics. Consequently, impurity removal efficiency is limited.

In the MG-Si with Mg alloying sample, the dominant precipitate becomes Mg_2Si, and it is widely spread at the grain boundaries, or in other words, as a secondary phase between the primary silicon grains. Meanwhile, many other insoluble phases, e.g., Fe-bearing silicide, are found embedded inside the Mg_2Si precipitate matrix. Subsequently, when the acid leaching process starts, the highly reactive Mg_2Si phase is dissolved into the acid solution. At the same time, the poorly leachable silicide, which is embedded in Mg_2Si precipitates, could also be carried away physically. In addition, the observed cracking effect due to the intensive exothermic reaction between Mg_2Si and aqueous HCl solution is also favorable to promote the kinetics of further impurity removal. Consequently, after sufficient leaching time, impurities can be effectively removed.

4.2. Effect of acid concentration

Although the entire acid leaching process of Mg-alloyed Si is a heterogeneous solid-state reaction, the governed reaction is expected to be the decomposition of Mg_2Si due to its principal amount. However, since a distinct maximum of impurity removal degree was observed, it

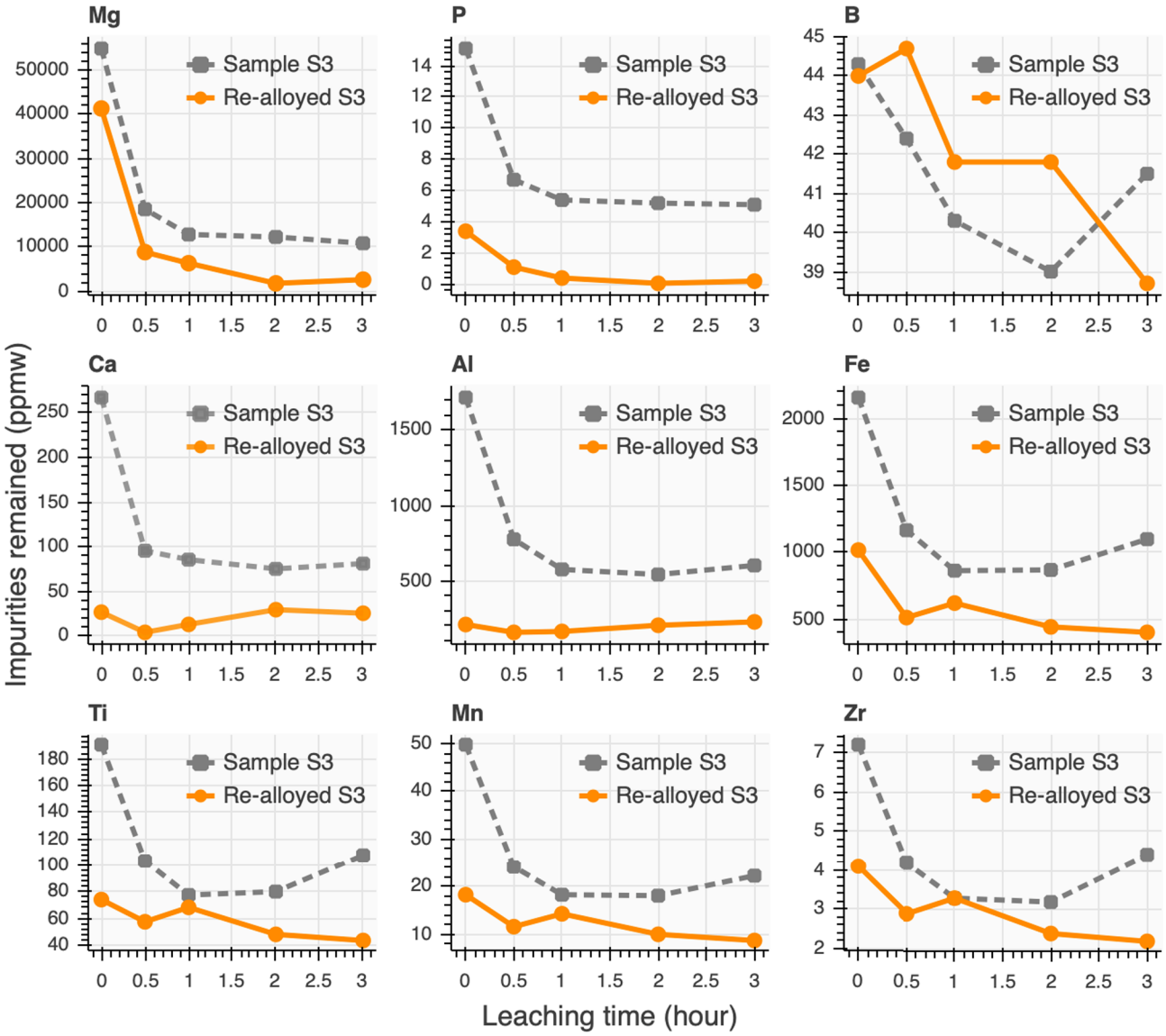

Fig. 6. Remained impurities concentration in leaching samples as a function of leaching time. Symbols show the measured concentrations of the leached samples S3 (L6-L9) and S3-leached sample that was re-alloyed by Mg and re-leached (L10-L13).

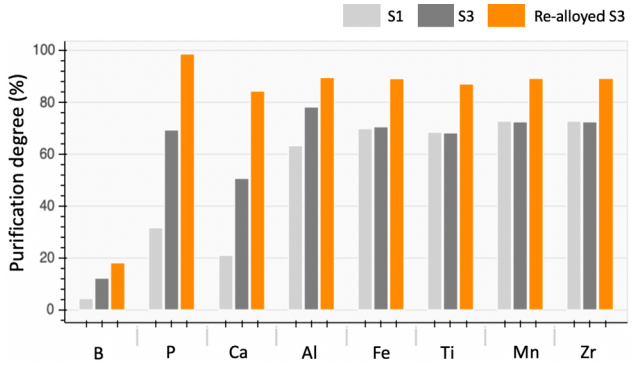

Fig. 7. Acid leaching purification efficiency comparison of sample S1 (MG-Si), S3 (Si-5.5 wt% Mg), and Re-alloyed S3.

implies that different factors govern the leaching process.

From the viewpoint of reaction kinetic factors, high concentration HCl solution is usually with high surface tension, which may suppress the chemical reaction located at micro pores. Consequently, with very high HCl concentration, the impurity removal degree in a given time decreased. On the other hand, from the viewpoint of the chemical reaction itself, the Mg_2Si decomposition in aqueous HCl is controlled by more complicated steps rather than HCl in the anhydrous condition which can be simply considered as [48]

$$Mg_2Si(s) + HCl(aq.) \rightarrow MgCl_2(aq.) + SiH_4(g) \quad (3)$$

The detailed reaction mechanism of Mg_2Si decomposition in aqueous HCl has been comprehensively investigated by Schwarz et al. [49]. It was found that the total reaction can be separated into several steps. Firstly, a primary hydrolysis reaction takes place and leads to the formation of an intermediate hydrolysis product dihydroxymagenesiosilane ($(HOMg)_2SiH_2$),

$$Mg_2Si + 2H_2O \xrightarrow{HCl} \begin{bmatrix} HO-Mg \\ HO-Mg \end{bmatrix} \diagup\!\!\diagdown SiH_2 \quad (4)$$

This intermediate is then further acidic hydrolyzed by breaking the two Mg-Si bonds and form silane gas:

$$\begin{bmatrix} HO-Mg \\ HO-Mg \end{bmatrix} \diagup\!\!\diagdown SiH_2 + 4HCl \rightarrow 2MgCl_2 + SiH_4 + 2H_2O \quad (5)$$

And also may result in the formation of some hydrogen gas:

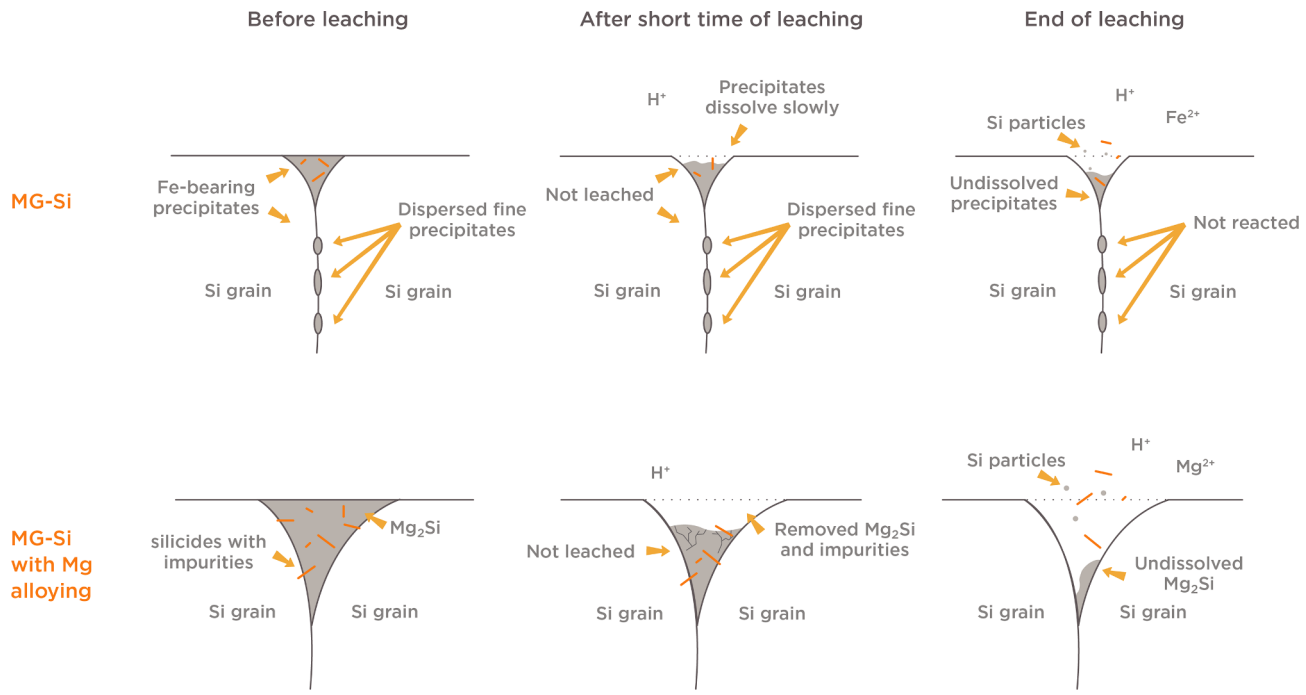

Fig. 8. Sketch of the impurity removal mechanism of MG-Si and Mg alloyed Si during acid leaching.

$$\begin{bmatrix} HO-Mg \\ HO-Mg \end{bmatrix} \diagdown SiH_2 + 2H_2O + 4HCl \rightarrow 2MgCl_2 + 4H_2 + SiO_2 \quad (6)$$

It can be seen that the total reaction of Mg_2Si decomposition is governed by both hydrolysis and reactive HCl acid interaction. On one hand, the primary hydrolysis reaction rate is determined by the amount of available H_2O in solution, which decreases with increasing HCl concentration. The total leaching efficiency is therefore limited under concentrated HCl condition. On the other hand, if the concentration of reactive HCl molecules becomes too low, the subsequent reactions will be suppressed as well and result in a lower leaching efficiency accordingly. While at the concentration of HCl around 10%, the optimum condition of the process is achieved, the acid leaching results thus exhibit a well-defined maximum observed in Fig. 5.

4.3. Enhancement of phosphorus segregation

In Section 3.2, it was confirmed by the SIMS mapping that the P segregation is evidently enhanced in the Si-Mg alloy system. Hence, the possible reasons for Mg alloying effects on P segregation enhancement are discussed below, respectively, from the liquidus variation based physical perspective and elements interactionbased chemical perspective.

- Physical perspective

P segregation coefficient in Si is defined as the ratio of P concentration in the solid phase and in the liquid phase during solidification, which is equivalent to the ratio of solidus line and liquidus line and can be calculated as:

$$k_P^{Si} = \frac{X_{Solidus,Si-P}}{X_{Liquidus,Si-P}} \quad (7)$$

where $X_{Solidus,Si-P}$ and $X_{Liquidus,Si-P}$ represent the molar concentrations of P in solid state and in liquid state of Si, respectively. The P segregation coefficient k_P^{Si} is well-known to be $k_P^{Si} = 0.35$ [47] for low P-containing Si-P alloys.

If one assumes there is no significant variation on the solidus line of P in Si after Mg addition (the interaction between Mg and P is ignored in solidified primary silicon due to the low concentration), and the very low concentration of P in Si-Mg alloys has no effect on the liquidus curve, the segregation coefficient of P in Si-Mg system then only relies on the change of liquidus line from Si-P system to Si-Mg system. Therefore, Eq. (7) can be written for the dilute solutions of P in Si-Mg-P system as:

$$k_P^{Si-Mg} = \frac{X_{Solidus,Si-P}}{X_{Liquidus,Si-Mg}} = \frac{X_{Solidus,Si-P}}{X_{Liquidus,Si-P}} \frac{X_{Liquidus,Si-P}}{X_{Liquidus,Si-Mg}} = k_P^{Si} \frac{X_{Liquidus,Si-P}}{X_{Liquidus,Si-Mg}} \quad (8)$$

where $X_{Liquidus,Si-Mg}$ represents the liquidus composition of Si-Mg system, and the term $\frac{X_{Liquidus,Si-P}}{X_{Liquidus,Si-Mg}}$ is regarded as the correction factor of k_P^{Si}. If $\frac{X_{Liquidus,Si-P}}{X_{Liquidus,Si-Mg}} < 1$, then the actual segregation coefficient of P is subsequently reduced from the theoretical 0.35 in Eq. (7).

The liquidus of binary Si-P and Si-Mg systems are plotted and compared at the Si-rich portion shown in Fig. 9. The Si-Mg liquidus line is obtained from the former work of Safarian et al.[50], and the Si-P liquidus is calculated by the same method based on the data in the Si-rich portion [51,52].

It can be seen from Fig. 9 that for a given temperature, the Si-Mg liquidus appears in the right side of Si-P liquidus. In other word, $X_{Liquidus,Si-P}$ is smaller than $X_{Liquidus,Si-Mg}$ at a given temperature, so we have $\frac{X_{Liquidus,Si-P}}{X_{Liquidus,Si-Mg}} < 1$. Therefore, the segregation coefficient of P is assumed to be reduced accordingly with the Mg alloying. However, it has to be noted that the liquidus variation assumption only works when Mg concentration is low because only in such case the interaction between Mg and P in Si melt can be ignored.

- Chemical perspective

From the chemical perspective, the segregation coefficient of P in Mg-alloyed Si can be obtained from the chemical potential equilibrium between the solid and liquid as the following equation:

$$\mu_{P \text{ in } Si(s)} = \mu_{P \text{ in } Si-Mg(l)} \quad (9)$$

where $\mu_{P \text{ in } Si(s)}$ and $\mu_{P \text{ in } Si-Mg(l)}$ are the chemical potential of P in primary solid Si front and in the liquid front.

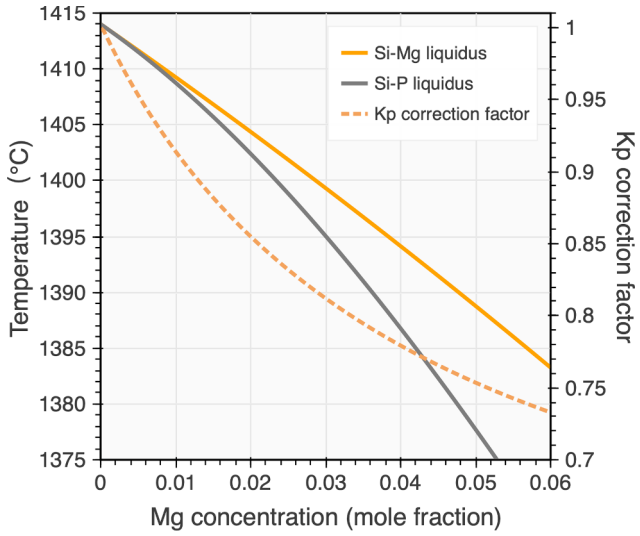

Fig. 9. Liquidus of Si-P and Si-Mg systems in the Si-rich portion and the correction factor changes.

Therefore,

$$RT\ln a_{\mathrm{P\ in\ Si}(s)} = RT\ln a_{\mathrm{P\ in\ Si-Mg}(l)} \tag{10}$$

where $a_{\mathrm{P\ in\ Si}(s)}$ and $a_{\mathrm{P\ in\ Si-Mg}(l)}$ are the activity of P in primary solid Si front and in the liquid front.

Based on the above equilibrium condition, it then gives

$$X_{\mathrm{P\ in\ Si}(s)}\gamma^0_{\mathrm{P\ in\ Si}(s)} = X_{\mathrm{P\ in\ Si-Mg}(l)}\gamma_{\mathrm{P\ in\ Si-Mg}(l)} \tag{11}$$

The segregation coefficient is then can be calculated as:

$$k_{\mathrm{P}}^{\mathrm{Si-Mg}} = \frac{X_{\mathrm{P\ in\ Si}(s)}}{X_{\mathrm{P\ in\ Si-Mg}(l)}} = \frac{\gamma_{\mathrm{P\ in\ Si-Mg}(l)}}{\gamma^0_{\mathrm{P\ in\ Si}(s)}} = \frac{\gamma^0_{\mathrm{P\ in\ Si}(l)}}{\gamma^0_{\mathrm{P\ in\ Si}(s)}}\frac{\gamma_{\mathrm{P\ in\ Si-Mg}(l)}}{\gamma^0_{\mathrm{P\ in\ Si}(l)}} = k_{\mathrm{P}}^{\mathrm{Si}}\frac{\gamma_{\mathrm{P\ in\ Si-Mg}(l)}}{\gamma^0_{\mathrm{P\ in\ Si}(l)}} \tag{12}$$

where $\gamma^0_{\mathrm{P\ in\ Si}(s)}$ and $\gamma^0_{\mathrm{P\ in\ Si}(l)}$ represent the activity coefficient of P in solid and liquid Si, $\gamma_{\mathrm{P\ in\ Si-Mg}(l)}$ represents the activity coefficient of P in Si-Mg melt. The above equation is obtained based on the fact that the two solid and liquid phases are at equilibrium and necessarily the chemical potential, or the chemical activity, of P in the two phases are equal. In principle, the activity coefficient of P in Si-Mg-P melt can be expressed as:

$$\ln\gamma_{\mathrm{P\ in\ Si-Mg}(l)} = \ln\gamma^0_{\mathrm{P\ in\ Si}(l)} + \varepsilon^{\mathrm{P}}_{\mathrm{P\ in\ Si}}X_{\mathrm{P\ in\ Si}(l)} + \varepsilon^{\mathrm{P}}_{\mathrm{Mg\ in\ Si}}X_{\mathrm{Mg\ in\ Si}(l)} \tag{13}$$

where $\varepsilon^{\mathrm{P}}_{\mathrm{Mg\ in\ Si}}$ represents the interaction coefficient of Mg and P in Si melt on each other. Parameter $\varepsilon^{\mathrm{P}}_{\mathrm{P\ in\ Si}}$ is the self-interaction coefficient of P, and the term $\varepsilon^{\mathrm{P}}_{\mathrm{P\ in\ Si}}X_{\mathrm{P\ in\ Si}(l)}$ can be ignored due to the ultra-low P concentration at ppmw level in the melt. Therefore, we have:

$$\ln\frac{\gamma_{\mathrm{P\ in\ Si-Mg}(l)}}{\gamma^0_{\mathrm{P\ in\ Si}(l)}} = \varepsilon^{\mathrm{P}}_{\mathrm{Mg\ in\ Si}}X_{\mathrm{Mg\ in\ Si}(l)} \tag{14}$$

Combining the above Eqs. (12) and (14), $k_{\mathrm{P}}^{\mathrm{Si-Mg}}$ can be rewritten as:

$$k_{\mathrm{P}}^{\mathrm{Si-Mg}} = k_{\mathrm{P}}^{\mathrm{Si}}\exp(\varepsilon^{\mathrm{P}}_{\mathrm{Mg\ in\ Si}}X_{\mathrm{Mg\ in\ Si}(l)}) \tag{15}$$

Since $X_{\mathrm{Mg\ in\ Si}(l)}$ is always larger than 0 in Si-Mg alloy system, and the sign of term $\varepsilon^{\mathrm{P}}_{\mathrm{Mg\ in\ Si}}$ is negative due to the widely known strong attraction of alkaline-earth element to P to form stable phosphide [53–55], it is expected that the segregation coefficient of P continuously decreases with increasing Mg addition into Si. The value of $\varepsilon^{\mathrm{P}}_{\mathrm{Mg\ in\ Si}}$ is later estimated to be as negative as −10.8 in present work in Section 4.4 and it confirms this explanation. Indeed, the enhancement of P segregation is thought due to the interaction and formation of some stable P-bearing clusters in the melt, suggested by the following two paths:

$$2\mathrm{P} + 1.5\mathrm{Mg_2Si} \rightarrow \mathrm{Mg_3P_2} + 1.5\mathrm{Si} \tag{16}$$

$$2\mathrm{SiP} + \mathrm{Mg_2Si} \rightarrow \mathrm{MgSiP_2} + \mathrm{Si} \tag{17}$$

Although P is known favorable to segregate at several specific sites in pure Si [56], it is expected that Mg addition attracts more P into the Mg_2Si precipitates, which are further easily removed in acid leaching and yielding higher P removal degree. The chemical interaction between Mg and P is considered the main reason for the successful P removal. Moreover, this interaction governs the P segregation enhancement during the whole solidification temperature-composition range.

4.4. Phosphorus removal modeling for Mg-doped silicon

The modeling method applied here refers to the methodology employed by Shimpo et al.[34]. The assumptions are made here as follows:

A1. The behavior of solute element during growth of primary silicon grains from the Mg-alloyed Si melts follows the Gulliver-Scheil equation, the diffusion of solute in solid Si can be ignored and the remaining liquid alloy is homogeneous.
A2. The secondary precipitates (eutectic phases) are completely removed in acid leaching step. Thus, the value of P content that is measured by ICP-MS after leaching is equivalent to the P in primary Si (solid solution) before the eutectic reaction starts.
A3. Thermodynamic properties of ultra-low P concentration at ppmw level are independent of temperature. Thus, the interaction parameter $\varepsilon^{\mathrm{P}}_{\mathrm{Mg\ in\ Si}}$ remains constant during the whole solidification range.

As illustrated in Fig. 10, the above assumptions yield P redistribution during solidification in solidified primary silicon grains and in the remained melt. It is seen that for a given initial P concentration $X^{initial}_{\mathrm{P\ in\ Si}(l)}$, the segregation starts from the beginning of primary Si grains formation and ends up to the beginning of the eutectic reaction. In addition, the concentration of P in solidified Si grains increases as the solid fraction increases. The trend becomes more rapidly at the final stage that is close to the eutectic point. The dotted lines plotted in the eutectic region are theoretically and experimentally approved concentration profile trend assuming no eutectic reaction (low P-containing Si-P melt solidification).

The theoretical P removal degree for the ternary system is defined here as Eq. (18):

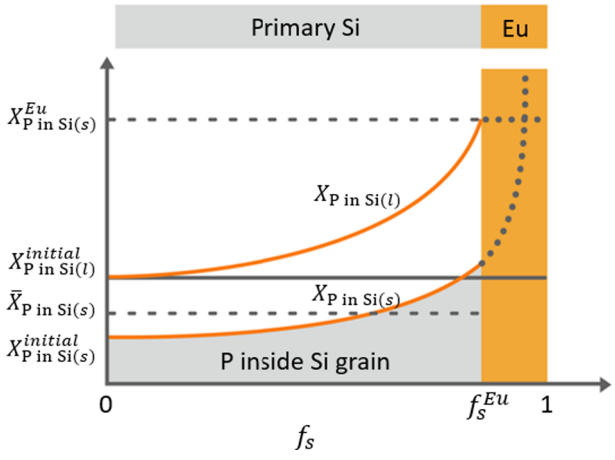

Fig. 10. Sketch of concentration profile of P in solidified primary silicon and the corresponding average P concentration in the remained melt and solidified eutectic portion.

$$\eta = \left(\frac{X_{\mathrm{P\ in\ Si}(l)}^{initial} - \bar{X}_{\mathrm{P\ in\ Si(s)}}}{X_{\mathrm{P\ in\ Si}(l)}^{initial}} \right) \times 100\% \tag{18}$$

where $X_{\mathrm{P\ in\ Si}(l)}^{initial}$ is the initial P concentration before the acid leaching, and $\bar{X}_{\mathrm{P\ in\ Si(s)}}$ is the average concentration of P segregated inside primary Si grain, and from mathematical point of view it is the shaded grey area under the $X_{\mathrm{P\ in\ Si}(s)}^{initial}$ curve in Fig. 10. The following mass balance is further applied to determine the value of $\bar{X}_{\mathrm{P\ in\ Si}(s)}$,

$$\bar{X}_{\mathrm{P\ in\ Si}(s)} f_s^{Eu} = \int_0^{f_s^{Eu}} X_{\mathrm{P\ in\ Si}(s)} df_s \tag{19}$$

where f_s is the solid fraction of primary Si, f_s^{Eu} is the primary Si solid fraction at the starting point of eutectic reaction, and $X_{\mathrm{P\ in\ Si}(s)}$ is the concentration of P at solid front which can be calculated as:

$$X_{\mathrm{P\ in\ Si}(s)} = k_{\mathrm{P}}^{\mathrm{Si-Mg}} X_{\mathrm{P\ in\ Si}(l)}^{initial} (1 - f_s)^{k_{\mathrm{P}}^{\mathrm{Si-Mg}} - 1} \tag{20}$$

By rearranging and integrating Eq. (20), the following relationship can be derived:

$$\bar{X}_{\mathrm{P\ in\ Si(s)}} = \frac{X_{\mathrm{P\ in\ Si}(l)}^{initial}}{f_s^{Eu}} \left(1 - (1 - f_s^{Eu})^{k_{\mathrm{P}}^{\mathrm{Si-Mg}}}\right) \tag{21}$$

Hence, combing Eqs. (18) and (21), we obtain:

$$\eta = \left(1 - \frac{1 - \frac{X_{\mathrm{P\ in\ Si}(l)}^{Eu}}{X_{\mathrm{P\ in\ Si}(l)}^{initial}} (1 - f_s^{Eu})}{f_s^{Eu}} \right) \times 100\% \tag{22}$$

The term $\frac{X_{\mathrm{P\ in\ Si}(l)}^{Eu}}{X_{\mathrm{P\ in\ Si}(l)}^{initial}}$ can be further obtained from Gulliver-Scheil equation that:

$$(1 - f_s) dX_{\mathrm{P}(l)} = (X_{\mathrm{P\ in\ Si}(l)} - X_{\mathrm{P\ in\ Si}(s)}) df_s \tag{23}$$

Considering the relationship $X_{\mathrm{P\ in\ Si}(s)} = k_{\mathrm{P}}^{\mathrm{Si-Mg}} X_{\mathrm{P\ in\ Si}(l)}$, it yields:

$$\frac{dX_{\mathrm{P}(l)}}{X_{\mathrm{P}(l)}} = \frac{1 - k_{\mathrm{P}}^{\mathrm{Si-Mg}}}{(1 - f_s)} df_s \tag{24}$$

Integrating Eq. (24) from solidification start point to the eutectic solidification starting point gives:

$$\ln \frac{X_{\mathrm{P\ in\ Si}(l)}^{Eu}}{X_{\mathrm{P\ in\ Si}(l)}^{initial}} = \int_0^{f_s^{Eu}} \frac{1 - k_{\mathrm{P}}^{\mathrm{Si-Mg}}}{1 - f_s} df_s \tag{25}$$

Since the relationship between segregation coefficient and f_s has been derived by Eq. (20), and the segregation coefficient of Mg in Si is very low, so that we can approximate $k_{\mathrm{Mg}}^{\mathrm{Si}} \approx 0$, for the liquid concentration $X_{\mathrm{Mg\ in\ Si}(l)}$, it can be calculated as:

$$X_{\mathrm{Mg\ in\ Si}(l)} = \frac{X_{\mathrm{Mg\ in\ Si}(l)}^{initial}}{(1 - f_s)} \tag{26}$$

Combining Eqs. (15) and (26) we obtain:

$$k_{\mathrm{P}}^{\mathrm{Si-Mg}} = k_{\mathrm{P}}^{\mathrm{Si}} \exp\left(\frac{\varepsilon_{\mathrm{Mg\ in\ Si}}^{\mathrm{P}} X_{\mathrm{Mg\ in\ Si}(l)}^{initial}}{(1 - f_s)} \right) \tag{27}$$

And therefore, we can re-write Eq. (25) as:

$$\ln \frac{X_{\mathrm{P}(l)}^{Eu}}{X_{\mathrm{P\ in\ Si}(l)}^{initial}} = \int_0^{f_s^{Eu}} \frac{1 - k_{\mathrm{P}}^{\mathrm{Si}} \exp\left(\frac{\varepsilon_{\mathrm{Mg\ in\ Si}}^{\mathrm{P}} X_{\mathrm{Mg\ in\ Si}(l)}^{initial}}{(1 - f_s)} \right)}{1 - f_s} df_s \tag{28}$$

Thus, integrating Eq. (28) over the whole primary Si solidification range gives the result:

$$\frac{X_{\mathrm{P}(l)}^{Eu}}{X_{\mathrm{P\ in\ Si}(l)}^{initial}} = \frac{\exp\left[k_{\mathrm{P}}^{\mathrm{Si}} \left(E_i\left(\frac{\varepsilon_{\mathrm{Mg\ in\ Si}}^{\mathrm{P}} X_{\mathrm{Mg\ in\ Si}(l)}^{initial}}{(1 - f_s^{Eu})} \right) - E_i(\varepsilon_{\mathrm{Mg\ in\ Si}}^{\mathrm{P}} X_{\mathrm{Mg\ in\ Si}(l)}^{initial}) \right) \right]}{1 - f_s} \tag{29}$$

where the $E_i(x)$ function is defined as the integral $E_i(x) = \int_{-\infty}^{x} \frac{e^t dt}{t}$. Hence, a formula of the theoretical P removal degree from a P-containing Si-Mg melt is obtained as:

$$\eta = \left(1 - \frac{1 - \frac{\exp\left(k_{\mathrm{P}}^{\mathrm{Si}} E_i\left(\frac{\varepsilon_{\mathrm{Mg\ in\ Si}}^{\mathrm{P}} X_{\mathrm{Mg\ in\ Si}(l)}^{initial}}{1 - f_s^{Eu}} \right) \right)}{\exp(k_{\mathrm{P}}^{\mathrm{Si}} E_i(\varepsilon_{\mathrm{Mg\ in\ Si}}^{\mathrm{P}} X_{\mathrm{Mg\ in\ Si}(l)}^{initial}))}}{f_s^{Eu}} \right) \times 100\% \tag{30}$$

Considering the solid fraction at eutectic temperature can be written as:

$$f_s^{Eu} = 1 - \frac{X_{\mathrm{Mg\ in\ Si}(l)}^{initial}}{0.4629} \tag{31}$$

where 0.4629 is the mole composition of Mg at Si-Mg eutectic point [57].

Combing Eqs. (30) and (31), a final P removal degree model for the dilute P solutions of Si-Mg-P alloys can be obtained:

$$\eta = \frac{0.4629 \frac{\exp(0.35 E_i(0.4629 \varepsilon_{\mathrm{Mg\ in\ Si}}^{\mathrm{P}}))}{\exp(0.35 E_i(X_{\mathrm{Mg\ in\ Si}(l)}^{initial} \varepsilon_{\mathrm{Mg\ in\ Si}}^{\mathrm{P}}))} - X_{\mathrm{Mg\ in\ Si}(l)}^{initial}}{0.4629 - X_{\mathrm{Mg\ in\ Si}(l)}^{initial}} \times 100\% \tag{32}$$

The obtained model here reveals clearly that there are only two independent variables that control the final P removal degree: the initial Mg content $X_{\mathrm{Mg\ in\ Si}(l)}^{initial}$, and the interaction coefficient $\varepsilon_{\mathrm{Mg\ in\ Si}}^{\mathrm{P}}$. Thus, for this two-parameter dependent relationship, if one variable is known, the other can be determined based on experimental results. In the present work, the Mg-P interaction coefficient $\varepsilon_{\mathrm{Mg\ in\ Si}}^{\mathrm{P}}$ is determined by fitting the experimental results from the leaching set (L14-L17) where the ultrasonic condition applied. This is because the acoustic cavitation effects [58] and more dispersed fine particles [59] make the ultrasonic leaching generally more efficient than magnetic stirring leaching. Thus, a near complete removal of the eutectic secondary precipitates can be achieved to better meet the assumption A2.

The plotted η against the amount of added Mg in Fig. 11 shows that the proposed P removal model tends to give predictions, which are in good agreement with existing results. Furthermore, $\varepsilon_{\mathrm{Mg\ in\ Si}}^{\mathrm{P}}$ is fitted to be -10.8. This negative value also confirms the strong chemical attraction of Mg to P in Si melt as discussed before in Section 4.3. Moreover, by employing Eq. (15), the relationship between Mg addition and P segregation coefficient variation can be further determined as Eq. (33) and it is shown in Fig. 12. Seeing that the segregation coefficient of P continuously decreases with Mg addition, the Mg addition is therefore expected to enhance the P removal in the applied process.

$$k_P^{\mathrm{Si-Mg}} = 0.35 \exp(-10.8 X_{\mathrm{Mg\ in\ Si}(l)}) \tag{33}$$

It is worth to note that the obtained P removal model here can be extended to more general scenarios for the leaching of other alloying systems in which silicon is doped by metal Me to obtain Si-Me alloy system in the Si-rich port. Hence, a more general model concentrates on the theoretical analysis of P removal degree by acid leaching of an arbitrary binary Si-Me eutectic alloy system can be written as:

$$\eta = \frac{X^{eu} \varphi(\varepsilon_{\mathrm{Me\ in\ Si}}^{\mathrm{P}}, X^{initial}) - X^{initial}}{X^{eu} - X^{initial}} \times 100\% \tag{34}$$

where $X^{initial}$ and X^{eu} are the alloying metal concentrations at initial and at the eutectic point. It is worth noting that for a specific alloy system, the X^{eu} is a constant. $\varepsilon_{\mathrm{Me\ in\ Si}}^{\mathrm{P}}$ indicates the Me-P interaction

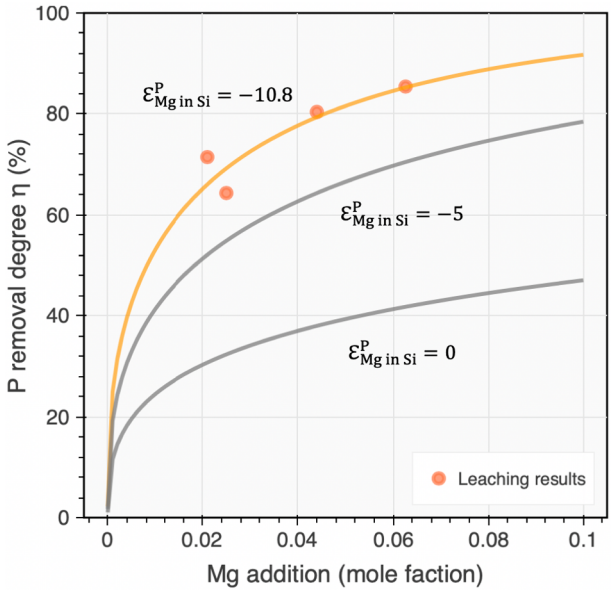

Fig. 11. Interaction parameter fitting results based on experimental results of leaching trials (L14-L17) and comparison of the estimated P removal degree as a function of Mg addition.

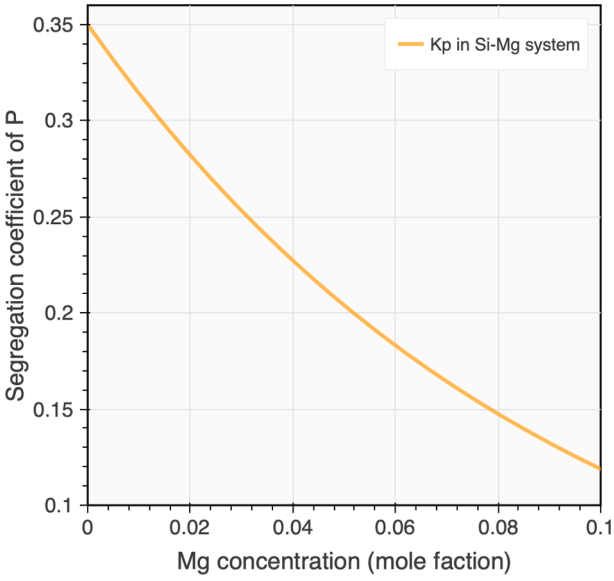

Fig. 12. Effect of Mg alloying concentration on the segregation coefficient of P in Si-Mg-P system.

coefficient, and the $\varphi(\varepsilon^{P}_{Me\ in\ Si}, X^{initial})$ is further defined as:

$$\varphi(\varepsilon^{P}_{Me\ in\ Si}, X^{initial}) = \frac{\exp(0.35E_i(\varepsilon^{P}_{Me\ in\ Si}X^{eu}))}{\exp(0.35E_i(\varepsilon^{P}_{Me\ in\ Si}X^{initial}))} \tag{35}$$

The above model also shows that P segregation in Si-Me binary system follows a two-parameter dependent relationship, further to say, the purification process is mainly controlled by interaction coefficient and the alloying concentration. Based on the present theoretical and experimental work, if one wants to achieve high P removal by the alloying method, the following strategies can be applied: (1) increase the alloying element amount, (2) adopt the alloying element with more negative interaction parameter value to P or bigger solid fraction at eutectic point, and (3) repeat the alloying-leaching process multiple times.

4.5. Effect of process operation times

In Section 3.5, it was observed that after a two-time Mg alloying-leaching process, P concentration could be further removed and meet the purity requirement of SoG-Si. For an arbitrary Si-Me system, if the averaged P segregation coefficient $\bar{k}_P^{Si-Me}$ during solidification is known, the relationship between P concentration before and after the first time alloying-leaching purification process can be directly obtained by rearranging Eq. (21) as:

$$\frac{\bar{X}_{P\ in\ Si(s)}}{X^{initial}_{P\ in\ Si(l)}} = \frac{(1-(1-f_S^{Eu})^{\bar{k}_P^{Si-Me}})}{f_S^{Eu}} \tag{36}$$

Considering the relation $f_S^{Eu} = 1 - f_L^{Eu}$, it yields:

$$\frac{\bar{X}_{P\ in\ Si(s)}}{X^{initial}_{P\ in\ Si(l)}} = \frac{1-f_L^{Eu\,\bar{k}_P^{Si-Me}}}{1-f_L^{Eu}} \tag{37}$$

So that,

$$\eta = \left(\frac{X^{initial}_{P\ in\ Si(l)} - \bar{X}_{P\ in\ Si(s)}}{X^{initial}_{P\ in\ Si(l)}}\right) \times 100\% = \frac{f_L^{Eu\,\bar{k}_P^{Si-Me}} - f_L^{Eu}}{1-f_L^{Eu}} \times 100\% \tag{38}$$

Thus, by considering the effect of multiple operation times into Eq. (38), the final P concentration after conducting the alloying-leaching process for n times can be written as:

$$\frac{\bar{X}^n_{P\ in\ Si(s)}}{X^{initial}_{P\ in\ Si(l)}} = \left(\frac{1-f_L^{Eu\,\bar{k}_P^{Si-Me}}}{1-f_L^{Eu}}\right)^n \tag{39}$$

where $\bar{X}^n_{P\ in\ Si(s)}$ is the final P concentration in Si after n times alloying-leaching process.

The above model offers another method to calculate the P removal degree and to calculate required process operation times based on the averaged P segregation coefficient $\bar{k}_P^{Si-Me}$ and liquid fraction at eutectic point f_L^{Eu}. Here, the $\bar{k}_P^{Si-Me}$ can be calculated as Eq. (40), by integrating the k_P^{Si-Me} from the initial alloying metal concentration to the eutectic temperature and divided by the composition range.

$$\bar{k}_P^{Si-Me} = \frac{k_P^{Si}\int_{X^{initial}_{Me\ in\ Si(l)}}^{X^{Eu}_{Me\ in\ Si(l)}} \exp(\varepsilon^{P}_{Me\ in\ Si}X_{Me\ in\ Si(l)})dX_{Me\ in\ Si(l)}}{(X^{Eu}_{Me\ in\ Si(l)} - X^{initial}_{Me\ in\ Si(l)})} \tag{40}$$

After solving Eq. (40), we have:

$$\bar{k}_P^{Si-Me} = \frac{k_P^{Si}\exp(\varepsilon^{P}_{Me\ in\ Si}X_{Me\ in\ Si(l)})}{\varepsilon^{P}_{Me\ in\ Si}(X^{Eu}_{Me\ in\ Si(l)} - X^{initial}_{Me\ in\ Si(l)})} \tag{41}$$

In present work, the averaged P segregation coefficient is calculated as:

$$\bar{k}_P^{Si-Me} = \frac{k_P^{Si}\exp(-10.8X_{Me\ in\ Si(l)})}{-10.8(X^{Eu}_{Me\ in\ Si(l)} - X^{initial}_{Me\ in\ Si(l)})} \tag{42}$$

If one assumes $\bar{X}^n_{P\ in\ Si(s)} = 0.3$, 0.5, and 1.0 ppmw are the target P purification level, the relationship among Mg alloying concentration, initial P concentration, and the process operation times can be subsequently obtained, as shown in Fig. 13.

It is seen in Fig. 13 that the required purification process times can be adjusted based on by varying the initial P concentration and Mg alloying concentration. For the most often scenarios, MG-Si can be purified to a target purification level by 1-time or 2-time Mg alloying-leaching process. With more restrict purification reequipments (lowering the target P concentration), this process window gets narrower. Higher process operation time ($n > 2$) is then required with small Mg addition and high initial P concentration.

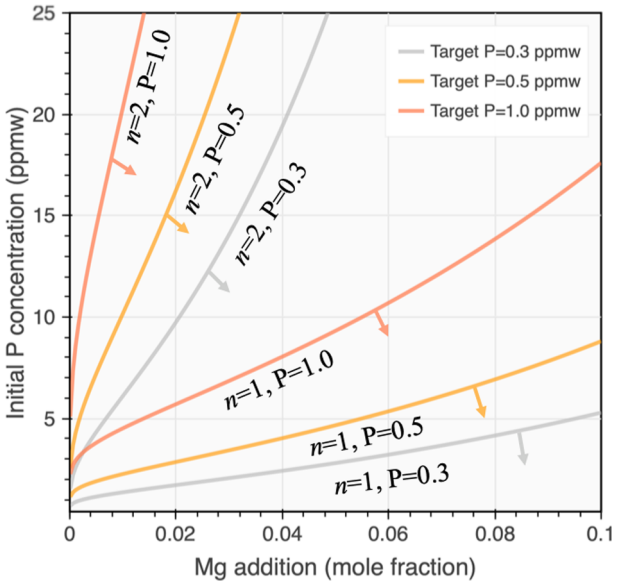

Fig. 13. A chart for the Mg alloying - acid leaching process; the initial P concentration before leaching (vertical axis), the target P concentration (on the curves), and the required Mg amount (horizontal axis) and the required operation times n (on the curves). Regions below the curve indicates the P concentration can be purified to the target level no more than n times.

5. Conclusions

In the present work, MG-Si purification by a combined process of Mg-alloying followed by HCl acid leaching was comprehensively investigated. The main conclusions can be summarized as:

(1) After Mg alloying, impurity-bearing phases were observed embedded inside the Mg_2Si eutectic precipitates and further removed to a large extent after acid leaching. The leaching efficiency of Mg alloyed MG-Si depends on acid concentration with an optimum as 10% HCl.
(2) A two times Mg alloying-leaching process was found able to effectively reduce P concentration from 15.1 ppmw to 0.2 ppmw, which meets the requirement of SoG-Si feedstock production.
(3) Enhancement of P segregation after Mg alloying was confirmed by SIMS mapping and thermodynamic analysis. The interaction coefficient $\varepsilon^{P}_{Mg\ in\ Si}$ was estimated to be -10.8.
(4) A theoretical model was developed for the P segregation of arbitrary low P-containing Si-Me-P alloy systems subjected to acid leaching process. The Si purification degree is dependent on the alloying metal concentration and the interaction coefficient between alloying metal Me to P.
(5) A process model was proposed by establishing the mathematical relationships among initial P concentration, target P concentration after purification, the amount of the alloying metal addition, and alloying-leaching operation times.

CRediT authorship contribution statement

Mengyi Zhu: Investigation, Validation, Visualization, Writing - original draft. **Alexander Azarov:** Investigation. **Eduard Monakhov:** Investigation. **Kai Tang:** Conceptualization. **Jafar Safarian:** Conceptualization, Methodology, Supervision, Project administration, Writing - review & editing.

Declaration of Competing Interest

The authors declare that they have no known competing financial interests or personal relationships that could have appeared to influence the work reported in this paper.

Acknowledgements

This work was performed at NTNU within the Research Centre for Sustainable Solar Cell Technology (FME SuSolTech, project number 257639), co-sponsored by the Norwegian Research Council and industry partners.

Appendix A. Supplementary material

Supplementary data to this article can be found online at https://doi.org/10.1016/j.seppur.2020.116614.

References

[1] A. Murgau, J. Safarian, Solar silicon production through metallurgical route and REC solar advancements, in: Silicon Chem. Sol. Ind. XIV, Svolvær, Norway, 2018, pp. 183–192.
[2] J. Safarian, M. Tangstad, Processes for upgrading metallurgical grade silicon to solar grade silicon, Energy Procedia 20 (2012) 88–97, https://doi.org/10.1016/J.EGYPRO.2012.03.011.
[3] N.P. Tucker, Preparation of high purity silicon, J. Iron Steel Ind. 15 (1927) 412–414.
[4] L.P. Hunt, V.D. Dosaj, J.R. McCormick, L.D. Crossman, Production of solar-grade silicon from purified metallurgical silicon, in: 12th IEEE Photovolt. Spec. Conf., 1976, pp. 125–129.
[5] J. Dietl, Hydrometallurgical purification of metallurgical-grade silicon, Sol. Cells 10 (1983) 145–154, https://doi.org/10.1016/0379-6787(83)90015-7.
[6] I.C. Santos, A.P. Goncalves, C.S. Santos, M. Almeida, M.H. Afonso, M.J. Cruz, Purification of metallurgical grade silicon by acid leaching, Hydrometallurgy 23 (1990) 237–246, https://doi.org/10.4028/www.scientific.net/AMR.418-420.1590.
[7] T.L. Chu, S.S. Chu, Partial purification of metallurgical silicon by acid extraction, J. Electrochem. Soc. 130 (1983) 455, https://doi.org/10.1149/1.2119730.
[8] J.C. Anglézio, C. Servant, F. Dubrous, Characterization of metallurgical grade silicon, J. Mater. Res. 5 (1990) 1894–1899, https://doi.org/10.1557/JMR.1990.1894.
[9] J.C. Anglezio, C. Servant, I. Ansara, Contribution to the experimental and thermodynamic assessment of the Al-Ca-Fe-Si system-I. Al-Ca-Fe, Al-Ca-Si, Al-Fe-Si and Ca-Fe-Si systems, Calphad 18 (1994) 273–309, https://doi.org/10.1016/0364-5916(94)90034-5.
[10] T. Margaria, J. Anglezio, C. Servant, Inlcrmetallic compounds in metallurgical silicon, in: Proc. 6th Int. Ferroalloys Congr., Cape Town, 1992, pp. 209–214.
[11] F. Margarido, J.P. Martins, M.O. Figueiredo, M.H. Bastos, Kinetics of acid leaching refining of an industrial Fe-Si alloy, Hydrometallurgy 34 (1993) 1–11, https://doi.org/10.1016/0304-386X(93)90077-Q.
[12] F. Margarido, M.H. Bastos, M.O. Figueiredo, J.P. Martins, The structural effect on the kinetics of acid leaching refining of Fe-Si alloys, Mater. Chem. Phys. 38 (1994) 342–347, https://doi.org/10.1016/0254-0584(94)90211-9.
[13] T. Yoshikawa, K. Morita, An evolving method for solar-grade silicon production: solvent refining, JOM 64 (2012) 946–951, https://doi.org/10.1007/s11837-012-0371-8.
[14] Y. Li, L. Zhang, Application of Si-based solvents to the purification of metallurgical grade-silicon, Sep. Purif. Rev. (2019) 1–24, https://doi.org/10.1080/15422119.2019.1623253.
[15] J.C. Jie, Q.C. Zou, J.L. Sun, Y.P. Lu, T.M. Wang, T.J. Li, Separation mechanism of the primary Si phase from the hypereutectic Al-Si alloy using a rotating magnetic field during solidification, Acta Mater. 72 (2014) 57–66, https://doi.org/10.1016/j.actamat.2014.03.031.
[16] T. Yoshikawa, K. Morita, Refining of silicon during its solidification from a Si–Al melt, J. Cryst. Growth. 311 (2009) 776–779, https://doi.org/10.1016/J.JCRYSGRO.2008.09.095.
[17] T. Yoshikawa, K. Morita, Refining of Si by the solidification of Si-Al melt with electromagnetic force, ISIJ Int. 45 (2005) 967–971, https://doi.org/10.2355/isijinternational.45.967.
[18] T. Yoshikawa, K. Morita, Removal of phosphorus by the solidification refining with Si-Al melts, Sci. Technol. Adv. Mater. 4 (2003) 531–537, https://doi.org/10.1016/j.stam.2003.12.007.
[19] Y. Li, Y. Tan, J. Li, K. Morita, Si purity control and separation from Si–Al alloy melt with Zn addition, J. Alloys Compd. 611 (2014) 267–272, https://doi.org/10.1016/J.JALLCOM.2014.05.138.
[20] T. Yoshikawa, K. Morita, An evolving method for solar-grade silicon production: solvent refining, n.d. doi: 10.1007/s11837-012-0371-8.
[21] Y. Lei, W. Ma, L. Sun, J. Wu, Y. Dai, K. Morita, Removal of B from Si by Hf addition during Al–Si solvent refining process, Sci. Technol. Adv. Mater. 17 (2016) 12–19, https://doi.org/10.1080/14686996.2016.1140303.
[22] Y. Li, B. Ban, J. Li, T. Zhang, X. Bai, J. Chen, S. Dai, Effect of cooling rate on phosphorus removal during Al-Si solvent refining, Metall. Mater. Trans. B 46 (2015) 542–544, https://doi.org/10.1007/s11663-015-0291-4.
[23] W. Yu, W. Ma, G. Lv, Y. Ren, Y. Dai, K. Morita, Low-cost process for silicon purification with bubble adsorption in Al-Si melt, Metall. Mater. Trans. B 45 (2014) 1573–1578, https://doi.org/10.1007/s11663-014-0050-y.
[24] J. Li, Y. Liu, Y. Tan, Y. Li, L. Zhang, S. Wu, P. Jia, Effect of tin addition on primary

silicon recovery in Si–Al melt during solidification refining of silicon, J. Cryst. Growth 371 (2013) 1–6, https://doi.org/10.1016/J.JCRYSGRO.2012.12.098.
[25] L. Hu, Z. Wang, X. Gong, Z. Guo, H. Zhang, Purification of metallurgical-grade silicon by Sn–Si refining system with calcium addition, Sep. Purif. Technol. 118 (2013) 699–703, https://doi.org/10.1016/J.SEPPUR.2013.08.013.
[26] X. Ma, T. Yoshikawa, K. Morita, Si growth by directional solidification of Si–Sn alloys to produce solar-grade Si, J. Cryst. Growth 377 (2013) 192–196, https://doi.org/10.1016/J.JCRYSGRO.2013.05.024.
[27] X. Ma, Y. Lei, T. Yoshikawa, B. Zhao, K. Morita, Effect of solidification conditions on the silicon growth and refining using Si–Sn melt, J. Cryst. Growth 430 (2015) 98–102, https://doi.org/10.1016/J.JCRYSGRO.2015.08.001.
[28] L. Zhang, Y. Ma, Y. Li, Preparing crystalline silicon from Si-Sn solvent by zone melting directional solidification method, Mater. Sci. Semicond. Process. 71 (2017) 12–19, https://doi.org/10.1016/J.MSSP.2017.06.044.
[29] K. Visnovec, C. Variawa, T. Utigard, A. Mitrašinović, Elimination of impurities from the surface of silicon using hydrochloric and nitric acid, Mater. Sci. Semicond. Process. 16 (2013) 106–110, https://doi.org/10.1016/j.mssp.2012.06.009.
[30] L. Huang, H. Lai, C. Lu, M. Fang, W. Ma, P. Xing, J. Li, X. Luo, Enhancement in extraction of boron and phosphorus from metallurgical grade silicon by copper alloying and aqua regia leaching, Hydrometallurgy 161 (2016) 14–21, https://doi.org/10.1016/j.hydromet.2016.01.013.
[31] L. Huang, A. Danaei, S. Thomas, P. Xing, J. Li, X. Luo, M. Barati, Solvent extraction of phosphorus from Si-Cu refining system with calcium addition, Sep. Purif. Technol. 204 (2018) 205–212, https://doi.org/10.1016/J.SEPPUR.2018.04.087.
[32] L.T. Khajavi, K. Morita, T. Yoshikawa, M. Barati, Removal of boron from silicon by solvent refining using ferrosilicon alloys, Metall. Mater. Trans. B. 46 (2015) 615–620, https://doi.org/10.1007/s11663-014-0236-3.
[33] A. Schei, High purity silicon production, in: Int. Semin. Refin. Alloy. Liq. Alum. Ferro-Alloys, Trondheim, Norway, 1985.
[34] T. Shimpo, T. Yoshikawa, K. Morita, Thermodynamic study of the effect of calcium on removal of phosphorus from silicon by acid leaching treatment, Metall. Mater. Trans. B 35 (2004) 277–284, https://doi.org/10.1007/s11663-004-0029-1.
[35] M.D. Johnston, M. Barati, Calcium and titanium as impurity getter metals in purification of silicon, Sep. Purif. Technol. 107 (2013) 129–134, https://doi.org/10.1016/j.seppur.2013.01.028.
[36] Y.V. Meteleva-Fischer, Y. Yang, R. Boom, B. Kraaijveld, H. Kuntzel, Slag treatment followed by acid leaching as a route to solar-grade silicon, Jom 64 (2012) 957–967, https://doi.org/10.1007/s11837-012-0383-4.
[37] Y.V. Meteleva-Fischer, Y. Yang, R. Boom, B. Kraaijveld, H. Kuntzel, Microstructure of metallurgical grade silicon during alloying refining with calcium, Intermetallics 25 (2012) 9–17, https://doi.org/10.1016/j.intermet.2012.02.009.
[38] Y.V. Meteleva-Fischer, Y. Yang, R. Boom, B. Kraaijveld, H. Kuntzel, Microstructure of metallurgical grade silicon and its acid leaching behaviour by alloying with calcium, Miner. Process. Extr. Metall. 122 (2013) 229–237, https://doi.org/10.1179/0371955313Z.00000000068.
[39] M. Fang, C. Lu, L. Huang, H. Lai, J. Chen, J. Li, W. Ma, P. Xing, X. Luo, Effect of calcium-based slag treatment on hydrometallurgical purification of metallurgical-grade silicon, Ind. Eng. Chem. Res. 53 (2014) 972–979, https://doi.org/10.1021/ie403047m.
[40] Y. Lei, W. Ma, X. Ma, J. Wu, K. Wei, S. Li, K. Morita, Leaching behaviors of impurities in metallurgical-grade silicon with hafnium addition, Hydrometallurgy 169 (2017) 433–439.
[41] Y. Lei, W. Ma, G. Lv, K. Wei, S. Li, K. Morita, Purification of metallurgical-grade silicon using zirconium as an impurity getter, Sep. Purif. Technol. 173 (2017) 364–371, https://doi.org/10.1016/j.seppur.2016.09.051.
[42] S. Espelien, G. Tranell, J. Safarian, Effect of magnesium addition on removal of impurities from silicon by hydrometallurgical treatment, in: Energy Technol. 2017, Springer, 2017, pp. 355–366.
[43] J. Safarian, S. Espelien, Hydrometallurgical purification of maganesium-doped silicon by difference acids, in: 33 Eur. Photovolt. Sol. Energy Conf. Exhib., 2017, pp. 480–482.
[44] M. Zhu, A. Murgau, J. Safarian, Effects of magnesium-doping on silicon leaching for solar grade feedstock production, in: 35th EU PVSEC 2018 Proc., 2018, pp. 465–468. doi: 10.4229/35thEUPVSEC20182018-2AV.1.3.
[45] J. Safarian, M. Tangstad, Vacuum refining of molten silicon, Metall. Mater. Trans. B Process Metall. Mater. Process. Sci. 43 (2012) 1427–1445, https://doi.org/10.1007/s11663-012-9728-1.
[46] A. Hoseinpur, K. Tang, J. Safarian, Kinetic study of vacuum evaporation of elements from ternary melts; case of dilute solution of P in Si-Al melts, Sep. Purif. Technol. 235 (2020), https://doi.org/10.1016/j.seppur.2019.116284.
[47] K. Morita, T. Miki, Thermodynamics of solar-grade-silicon refining, Intermetallics 11 (2003) 1111–1117, https://doi.org/10.1016/S0966-9795(03)00148-1.
[48] F. Fehér, W. Tromm, Die Darstellung von Silanen aus Magnesiumsilicid und Hydrazoniumchlorid in wasserfreiem Hydrazin, Zeitschrift Für Anorg. Und Allg. Chemie. 282 (1955) 29–40, https://doi.org/10.1002/zaac.19552820107.
[49] R. Schwarz, E. Konrad, Über den Reaktionsmechanismus der Silan-Bildung aus Magnesiumsilicid (I.), Berichte Der Dtsch, Chem. Gesellschaft (A B Ser.) 55 (1922) 3242–3252, https://doi.org/10.1002/cber.19220550938.
[50] J. Safarian, L. Kolbeinsen, M. Tangstad, Liquidus of Silicon Binary Systems, Metall. Mater. Trans. B 42 (2011) 852–874, https://doi.org/10.1007/s11663-011-9507-4.
[51] S. Liang, R. Schmid-Fetzer, Modeling of Thermodynamic Properties and Phase Equilibria of the Si-P System, J. Phase Equilibria Diffus. 35 (2014) 24–35, https://doi.org/10.1007/s11669-013-0269-3.
[52] J. Safarian, M. Tangstad, Phase diagram study of the Si-P system in Si-rich region, J. Mater. Res. 26 (2011) 1494–1503, https://doi.org/10.1557/jmr.2011.130.
[53] M.E. Schlesinger, The thermodynamic properties of phosphorus and solid binary phosphides, Chem. Rev. 102 (2002) 4267–4302, https://doi.org/10.1021/cr000039m.
[54] A.I. Zaitsev, N.V. Korolyov, B.M. Mogutnov, Thermodynamic properties of {xCa + (1–x)P}, J. Chem. Thermodyn. 23 (1991) 11–23, https://doi.org/10.1016/S0021-9614(05)80053-9.
[55] Z.V. Dobrokhotova, A.I. Zaitsev, M.A. Zemchenko, A.D. Litvina, B.M. Mogutnov, S.N. Yaschenko, Thermodynamic properties of calcium and barium phosphides, J. Therm. Anal. 38 (1992) 1113–1122, https://doi.org/10.1007/BF01979173.
[56] D. Zhao, Y. Li, Revealing the factors influencing grain boundary segregation of P, As in Si: Insights from first-principles, Acta Mater. 168 (2019) 52–62, https://doi.org/10.1016/J.ACTAMAT.2019.02.014.
[57] S. Liang, P. Wang, R. Schmid-Fetzer, Inherently consistent temperature function for interaction parameters demonstrated for the Mg-Si assessment, Calphad Comput. Coupling Phase Diagrams Thermochem. 54 (2016) 82–96, https://doi.org/10.1016/j.calphad.2016.06.003.
[58] X. Ma, J. Zhang, T. Wang, T. Li, Hydrometallurgical purification of metallurgical grade silicon, Rare Met. 28 (2009) 221–225, https://doi.org/10.1007/s12598-009-0043-1.
[59] S. Liu, K. Huang, H. Zhu, Removal of Fe, B and P impurities by enhanced separation technique from silicon-rich powder of the multi-wire sawing slurry, Chem. Eng. J. 299 (2016) 276–281, https://doi.org/10.1016/J.CEJ.2016.04.081.